Theoretical Study of the CF 2 CH 2 → HF + CF ⋮ CH Reaction

ARTICLE *in* THE JOURNAL OF PHYSICAL CHEMISTRY A · OCTOBER 2000

Impact Factor: 2.69 · DOI: 10.1021/jp001308f

Theoretical Study of the $CF_2{=}CH_2 \rightarrow HF + CF{\equiv}CH$ Reaction

Alexander M. da Silva, Graciela Arbilla,* and Edilson C. da Silva

Departamento de Físico-Química, Instituto de Química, Universidade Federal do Rio de Janeiro, Cidade Universitária, Rio de Janeiro, RJ, 21949-900 Brazil

Received: April 4, 2000; In Final Form: July 19, 2000

The stationary points for the four-center HF elimination reaction from the $CF_2{=}CH_2$ molecule have been obtained at different levels of ab initio (MP2, CISD, and MCSCF) and DFT calculations. The computed barrier heights are in good agreement with the experimental activation energy. The reaction path for this reaction has been traced and the coupling between the reaction coordinate and normal modes analyzed along it. The rate coefficients have been calculated for the temperature range 1000−1500 K using the canonical variational transition state theory. The calculated rate coefficients show good agreement with the experimental results.

Introduction

The fluorinated hydrocarbon compounds are efficient agents for depleting stratospheric ozone, and due to this property these compounds have been the subject of extensive experimental studies. Burgess et al.[1] reported a fundamental study for understanding the chemistry of these agents in hydrocarbon flames and proposed a chemical mechanism on the basis of the elementary reaction steps of fluoromethanes and fluorethanes. In that mechanism, the 1,1-difluoroethylene (1,1-DFE) reacts by addition of hydrogen atoms, followed by stabilization of the fluoroethyl radical produced, $CH_2{=}CF_2 + H \rightarrow CH_3CF_2^{\cdot}$ or $CHF_2CH_2^{\cdot}$, as well as fluorine atom elimination, $CH_2{=}CF_2 + H \rightarrow CH_2{=}CHF + F^{\cdot}$. Another way of depleting the fluoromethanes and fluorethanes is the reaction with oxygen,[1,2] $CH_2{=}CF_2 + O \rightarrow CHF_2 + HCO$, and OH, $CH_2{=}CF_2 + OH \rightarrow CH{=}CF_2 + H_2O$.

It has been proposed that the 1,1-DFE can be thermally decomposed by three possible channels of reaction: a two-step reaction involving the vinylidene or fluorovinylidene intermediate which rearranges to acetylene or fluroacetylene; the H or F migration leading to fluoroethylidene intermediates, which dissociate to give the products via a three-center type elimination; a concerted mechanism involving one cyclic transition state of the four members, i.e., of α, β, or four-center reaction.[3] The experimental results obtained by Simmie and Tschuikow-Roux[4] suggest the third mechanism to be the most probable one. Their results were obtained over the range 1287−1482 K and show a variation of the first-order rate coefficient with temperature according to the expression $\log(k) = (14.4 \pm 1.1) - (86 \pm 7)/2.3RT$, with an Arrhenius activation energy of 86 kcal mol^{-1}. Their work complements the kinetic data for the elimination reaction of halohydrocarbons.[5] Furthermore, the 1,1- and 1,2-isomers were targets of photolysis studies in the 1970s and 1980s. In these studies, the vibrationally excited HF is the prevailing photolysis product.[6−9]

To our knowledge, there is no theoretical study of the thermal decomposition of 1,1-DFE in the literature. Only the reaction paths of the elimination reactions of chloride compounds, C_2H_2-Cl_2, have been theoretically investigated.[10,11]

In this work, the reaction path and the rate coefficients for the four-center elimination of HF have been studied. The reaction path has been calculated using the intrinsic reaction coordinate (IRC)[12] approach. Following the methodology proposed by Truhlar et al.,[13] high-level electronic structure results have been used as input for variational transition state theory (VTST) calculations.

Ab initio and DFT calculations of the reaction path have been performed at different levels and using distinct sets of basis functions. In this way, the influence of the level of treatment of electron correlation and the quality of the basis employed on the kinetic results has been also investigated. The other proposed channels of reaction have been also investigated, but the calculated energy barrier were much higher than the experimental activation energy.[14]

Methods and Computational Details

Geometries, energies, and first and second energy derivatives have been computed using the GAUSSIAN 94[15] and GAMESS[16] electronic structure codes. The stationary point geometries (reactants, products, and saddle point) have been optimized at the following levels: restricted second-order MØller−Plesset perturbation theory,[17] MP2; B3LYP[18] and B3PW91[19] functionals; configuration interaction with singles and doubles substitutions,[20] CISD; multiconfigurational self-consistent field,[21] MCSCF. In this work, we have performed an MCSCF(2,6) calculation, i.e., singles and doubles substitutions in an active space composed of six orbitals, three occupied and three virtual. The occupied orbitals are two σ orbitals of the C−H and C−F bonds and a π orbital of the C≡C bond. This calculation will be denoted here in after by MC-2. Three basis sets have been used in the calculation: Huzinage−Dunning double-ζ valence basis set, with d polarization functions on each carbon and fluorine atoms and p functions on hydrogen, D95V(d,p);[22] this same basis augmented with one diffuse function, D95V++(d,p); the cc-pVTZ[23] Dunning's basis set. These bases will be denoted by B1, B2, and B3, respectively.

If one starts from the saddle-point geometry and goes downhill to both the asymptotic reactant and product channels in mass-weighted Cartesian coordinates, the IRC (intrinsic reaction coordinate) has been constructed at these different levels, with a gradient step size of 0.03 bohr amu$^{1/2}$. This value is small enough to provide convergence of the reaction path.

10.1021/jp001308f CCC: $19.00
Published on Web 09/28/2000

TABLE 1: Geometric Parameters of 1,1-DFE, HF, FCCH, and Saddle Point (*r*, Å; *θ*, deg)

	MP2		B3PW91			B3LYP				
parameter	B1	B2	B1	B2	B3	B1	B2	B3	Exp1	Exp2
					1,1-DFE					
R(CH)	1.079	1.079	1.082	1.082	1.078	1.082	1.083	1.077	1.079[a]	1.075[b]
R(CF)	1.331	1.332	1.324	1.324	1.317	1.329	1.330	1.322	1.323	1.324
R(CC)	1.334	1.334	1.327	1.327	1.316	1.328	1.328	1.315	1.315	1.316
θ(HCH)	121.3	121.4	120.7	120.7	120.5	120.6	120.6	120.5	121.9	119.3
θ(FCF)	109.6	109.6	109.7	109.6	109.7	109.6	109.5	109.6	109.1	109.7
					HF					
R(HF)	0.9237	0.9258	0.9249	0.9260	0.9197	0.9281	0.9294	0.9221	0.9168[c]	
					FCCH					
R(CH)	1.064	1.065	1.067	1.068	1.061	1.067	1.068	1.060	1.053[d]	
R(CF)	1.293	1.294	1.281	1.281	1.273	1.285	1.286	1.278	1.279	
R(CC)	1.220	1.219	1.206	1.206	1.192	1.206	1.206	1.192	1.198	
					Saddle Point					
$R(C_2F_1)$	1.289	1.287	1.280	1.276	1.268	1.283	1.279	1.270		
$R(C_2F_2)$	1.804	1.834	1.822	1.853	1.839	1.833	1.870	1.857		
$R(C_2C_1)$	1.263	1.263	1.261	1.260	1.248	1.263	1.262	1.248		
$R(C_1H_1)$	1.072	1.072	1.077	1.077	1.248	1.077	1.077	1.248		
$R(C_1H_2)$	1.400	1.378	1.425	1.398	1.396	1.421	1.391	1.386		
$R(H_2F_2)$	1.185	1.207	1.160	1.182	1.187	1.173	1.197	1.205		
$\theta(H_1C_1H_2)$	143.4	142.2	146.4	145.3	144.8	146.3	144.2	143.9		
$\theta(F_1C_2F_2)$	99.9	99.6	100.6	100.4	100.2	100.8	100.5	100.5		

[a] Experimental results from ref 27. [b] Experimental results from ref 28. [c] Experimental results from ref 29. [d] Experimental results from ref 30.

Smaller step sizes require an increase in computational effort without providing any noticiable difference in the results.[14] Along this minimum energy path (MEP), the reaction coordinate *s* is defined as the signed distance from the saddle-point, with $s > 0$ referring to the product side. Eight points in each direction plus the three stationary points have been selected on the MEP. The matrix of force constants has been computed and a generalized normal-mode analysis performed by projecting out frequencies at each point.[24] By using this information, the vibrational partition function along the MEP and the ground-state vibrationally adiabatic potential curve have been obtained; the latter is calculated by the following expression:

$$V_a^G(s) = V_{MEP(s)} + \epsilon_{int(s)}^G$$

Here $V_{MEP(s)}$ is the classical energy along the MEP with its zero energy at the reactants and $\epsilon_{int(s)}^G$ is the zero point energy at *s* evaluated from the generalized normal-mode vibrations orthogonal to the reaction coordinate.

The optimized geometries, energies, and first and second energy derivatives of these points on the MEP have been used to calculate the variational rate coefficients using the general polyatomic rate coefficients code POLYRATE.[25] In this work, the following approaches to the calculation of rate coefficients[26] have been used: conventional transition state theory (TST); canonical variational transition state theory (CVT); improved canonical variational theory (ICVT).

Results and Discussion

Stationary Points. The geometric parameters of reactant, products, and saddle point obtained at MP2 and DFT levels of theory are listed in Table 1. It can be seen in this table that these values show good agreement with experimental data (calculated values differ in less than 2% from experimental data). The errors are minimized by using basis set B3 (with the exception of the *r*(CF) bond length at B3PW91 calculation).

The saddle point structure is planar and of C_s symmetry at all levels of calculation, as shown in Figure 1. Its geometry is similar to the saddle point geometry in the HCl elimination from 1,1-dichloroethylene, described in ref 10. Assuming a one-step mechanism, the reaction leads directly to the products, hydrogen fluoride and fluoroacetylene. As shown in Figure 1, the reacting C−F bond is already very stretched and is virtually broken. The reacting C−H bond is only slightly stretched, and the HF bond is still substantially longer than in a free HF molecule. By comparison of the geometries of 1,1-DFE and that of the saddle point, it can be noticed that the C2−F2 bond length increases by about 36%, the length of the C1−H2 increases by 30%, and the length of the H2−F2 is 28% longer than in an HF molecule.

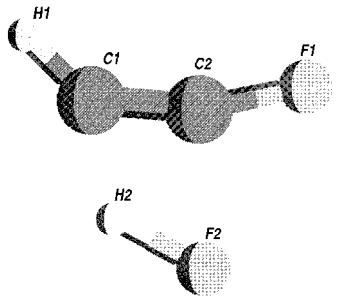

Figure 1. Geometry of the saddle point.

TABLE 2: Saddle Point Energy (Relative to 1,1-DFE), Zero Point Correction, and Critical Energy[a]

level calculation	saddle point	ZPC	E_0
MP2/B1	92.3	−5.2	87.1
/B2	91.1	−5.2	85.9
B3PW91/B1	89.8	−5.1	84.7
/B2	88.8	−5.2	83.6
/B3	88.2	−5.1	83.1
B3LYP/B1	89.5	−5.1	84.4
/B2	88.3	−5.2	83.1
/B3	88.2	−5.1	83.1
CISD/B1	101.8	−5.3	96.5
MC-2/B1	83.6	−5.0	78.6
CCSD(T)/B1	94.4	−5.1	89.4
MP4SDQ/B1	96.4	−5.3	91.1
Exp3			86 ± 7

[a] All values in kcal/mol. The experimental value is the Arrhenius activation energy (see text for details).

TABLE 3: Harmonic Vibrational Frequencies (cm^{-1}) of 1,1-DFE Calculated at the MP2, B3PW91, and B3LYP Levels Using the B1, B2, and B3 Bases Set

sym species	MP2		B3PW91			B3LYP			exptl[a]
	B1	B2	B1	B2	B3	B1	B2	B3	
A_1	3291.1	3288.2	3227.9	3223.1	3202.9	3213.4	3206.9	3195.3	ν_1 **3057.3 (*ν*(CH))**
A_1	1787.6	1777.6	1789.2	1783.1	1784.1	1776.0	1768.5	1774.2	ν_2 **1727.6 (*ν*(C═C))**
A_1	1443.8	1439.8	1404.4	1402.7	1404.3	1410.2	1408.0	1414.1	ν_3 1412.4 ($\delta(CH_2)$)
A_1	937.6	932.4	949.1	945.6	950.1	937.3	932.2	938.9	ν_4 925.5 (ν(CF))
A_1	545.9	519.6	548.6	548.0	555.6	543.6	542.2	551.1	ν_5 549.7 ($\delta(CF_2)$)
A_2	727.2	675.7	712.1	712.5	719.8	710.9	711.5	721.3	ν_6 592.0 (twist)
B_1	3419.2	3411.9	3338.8	3332.3	3305.8	3322.4	3313.7	3294.5	ν_7 3174.0 (ν(CH))
B_1	1344.4	1331.8	1344.1	1332.5	1325.7	1326.3	1310.8	1307.7	ν_8 1300.8 (ν(CF))
B_1	975.4	971.9	960.2	957.7	959.8	960.8	957.7	962.3	ν_9 954.3 (rock CH_2)
B_1	434.5	434.3	437.5	436.3	440.8	437.7	436.1	442.0	ν_{10} 437.0 (rock CF_2)
B_2	751.7	718.0	814.5	827.7	822.4	823.0	839.6	831.4	ν_{11} 802.1 (wag CH_2)
B_2	614.4	542.7	627.6	621.9	644.3	618.4	611.6	635.5	ν_{12} 609.6 (wag CF_2)

[a] Reference 31.

TABLE 4: Harmonic Vibrational Frequencies (cm^{-1}) of Saddle Points, Calculated at the MP2, B3PW91, and B3LYP Levels Using the B1, B2, and B3 Bases Set

	MP2		B3PW91			B3LYP		
	B1	B2	B1	B2	B3	B1	B2	B3
ν^*_1(A')	−1942.7	−1954.0	−1640.9	−1689.2	−1723.9	−1707.1	−1755.0	−1797.8
ν^*_2(A')	362.1	346.6	341.2	325.3	338.5	331.8	311.6	324.5
ν^*_4(A')	626.4	614.9	660.7	654.4	672.1	666.0	656.5	675.9
ν^*_5(A')	929.9	875.7	944.3	942.4	935.2	946.2	948.3	938.9
ν^*_6(A')	1049.4	1045.6	1062.9	1061.9	1069.5	1049.7	1048.1	1058.5
ν^*_7(A')	1787.4	1767.1	1779.9	1762.7	1758.6	1766.8	1747.9	1743.3
ν^*_8(A')	2064.1	2062.6	2058.2	2058.7	2060.1	2036.1	2039.9	2044.8
ν^*_9(A')	3447.6	3442.1	3366.2	3359.7	3349.5	3348.9	3342.8	3338.7
ν^*_{10}(A'')	434.8	397.6	419.4	405.9	442.1	407.1	393.1	430.4
ν^*_{11}(A'')	587.3	553.0	596.4	591.1	598.5	593.0	587.7	595.4
ν^*_{12}(A'')	789.1	744.1	795.9	760.2	764.5	784.4	748.1	757.2

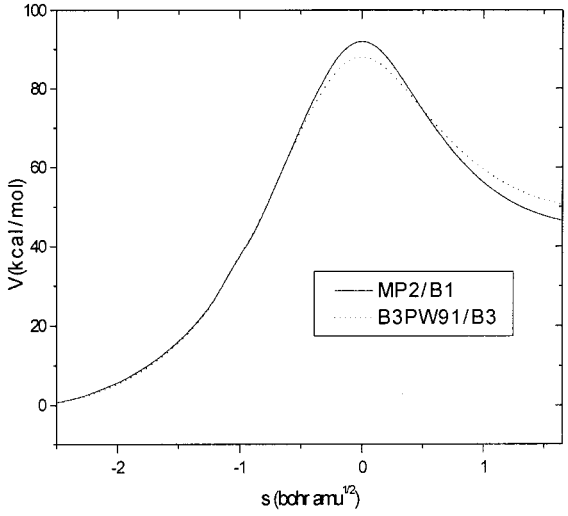

Figure 2. Reaction coordinate calculated at the MP2/B1 and B3PW91/B3 levels.

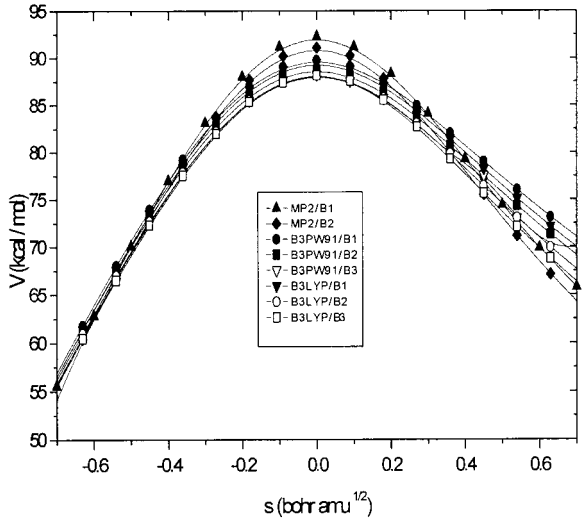

Figure 3. Reactions path, calculated at several levels, in the region of the saddle point. At all levels, the saddle point was arbitrarily localized at $s = 0$.

The energy of the saddle point relative to the 1,1-DFE, the zero point correction, and the critical energy, at several levels of calculation, are shown in Table 2. As known, the experimental activation energy, obtained from an Arrhenius plot, and shown in the last line of Table 2, is not exactly the same as the difference between the electronic energies of the saddle point and the reactant molecule. For a unimolecular reaction, to a very good approximation, this relation can be set as: $E_a = E_0 + RT$. For temperatures between 1000 and 1500 K, this correction lies between 2 and 3 kcal/mol. Therefore, the results for the MP2 and DFT calculations are in acceptable agreement with the experimental value (86 ± 7) kcal/mol for the Arrhenius activation energy. The B3PW91 and B3LYP results are similar to the MP2 values for the reaction barrier, and considering the experimental uncertainty, the differences are probably not meaningful. The results obtained by optimizing the wave function at CCSD(T) and MP4SDQ are shown only to demonstrate the efficiency of DFT and MP2 methods in the calculation of the reaction barrier; e.g., these methods are as efficient as methods of high computational cost. The reaction coordinate has not been obtained at CCSD(T) and MP4SDQ because the other methods are much faster than these ones, with similar results. The CISD calculation yields the worst value for the barrier height. One possible reason for the latter result is the lack of size consistency of the CISD wave function. The

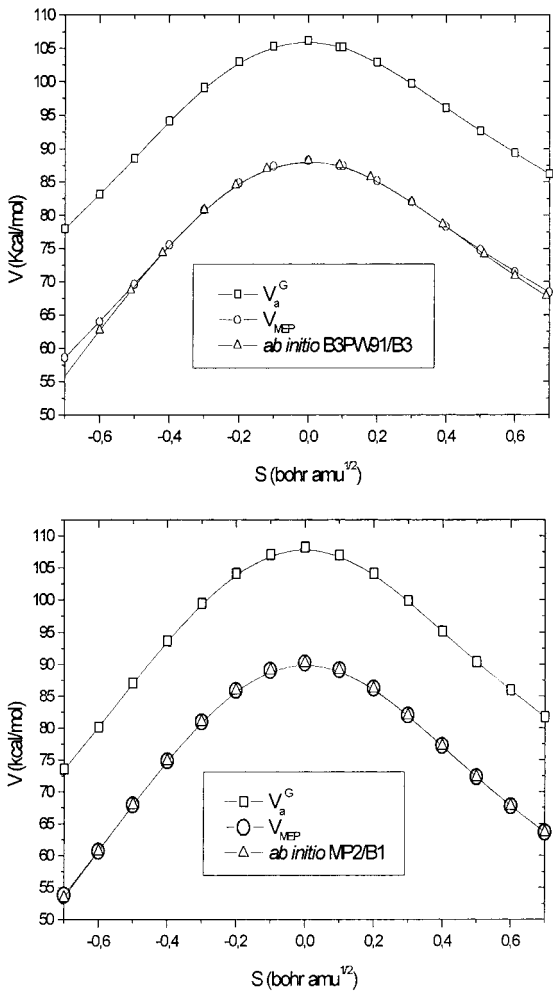

Figure 4. Classical potential energy curve (V_{MEP}) and vibrationally adiabatic potential energy curve (V_a^G) as a function of the distance along the MEP. The ab initio results are included for comparison.

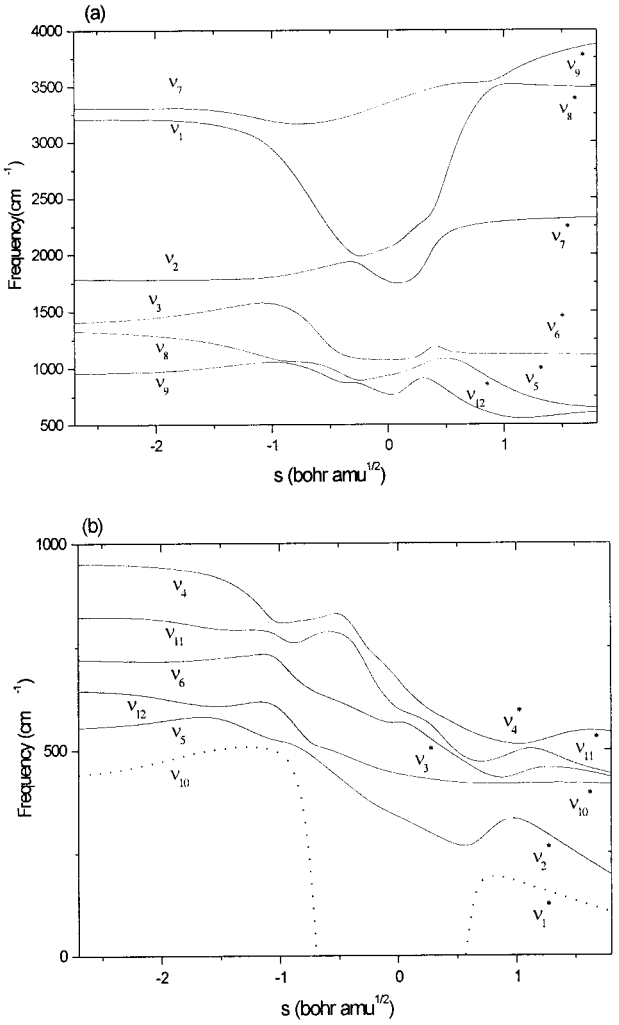

Figure 5. Variation of the generalized normal mode vibrational frequencies as a function of the reaction coordinate *s* at B3PW91/B3.

result would be improved by the inclusion of configurations containing higher-order replacements, providing the required flexibility of the wave function to describe the process of bond breaking and formation. It is important to stress that the above discussion comparing the performance of different levels of calculation is carried out within basis B1. As the computation costs scale as a power of the number of basis functions, calculations at levels other than MP2 or DFT have not been performed using bases B2 and B3.

Tables 3 and 4 show the frequencies of 1,1-DFE and saddle point, respectively, obtained at the MP2, B3PW91, and B3LYP levels using the B1, B2, and B3 bases. The results for 1,1-DFE are about 10% above the experimental values,[31] except for the vibrational mode A_2 twist where these results are about 20% above the experimental value, but this mode is active only in the Raman spectrum.[31]

The reaction coordinate has also been obtained at MC-2 and CISD as well as the rate coefficients (using basis B1 only), but these results will not be presented here.

Reaction Path. Figure 2 shows the reaction path at two levels of calculation, MP2/B1 and B3PW91/B3. Figure 3 shows all the reaction paths at the MP2, B3PW91, and B3LYP levels, in the region near the saddle point. In this figure, the influence of the level of calculation and the basis set used on the barrier height can be seen. From the figure it is noticed that the barrier is lowered by changing the calculation level in the order MP2, B3LYP, and B3PW91 and by changing the basis set.

Figure 4 shows the minimum energy path, V_{MEP}, and the ground-state vibrationally adiabatic potential energy surface, V_a^G, obtained by fitting the theoretically calculated (B3PW91/B3 and MP2/B1) points. The V_{MEP} curve and the ab initio curves are not exactly the same since the first one was obtained using POLYRATE computational code, by fitting the electronic structure data (energy and vibrational frequency data as a function of *s* values) to a continuous function. Figure 5 shows the variation of the generalized normal-mode frequencies along the reaction path obtained at the B3PW91/B3 level. In the negative limit of *s* ($s = -\infty$), there are 12 frequencies corresponding to 1,1-DFE. In the region of the saddle point, the reaction coordinate is composed of a complex mixture of the normal-mode frequencies. On the reactant side, it correlates with the CF_2 asymmetric bending in the plane, while on the product side it is composed by HF and CFCH fragment rotations. The other modes are also shown in this figure.

The change in the geometric parameters of 1,1-DFE obtained at the B3PW91/B3 level during the reaction is shown in Figure 6. Figure 6a shows the rupture of C1−H2 and C2−F2 bonds, formation of H2−F2, and conversion of the double bond to triple bond C1−C2. The distance between these atoms falls sharply close to the saddle point region due to angular distortion of the CH_2 and the CF_2 groups, as shown in Figure 6b. The CH_2 group shifts sooner than CF_2 along the reaction path. The double bond is monotonically converted to the triple bond $C_1{\equiv}C_2$ during the reaction.

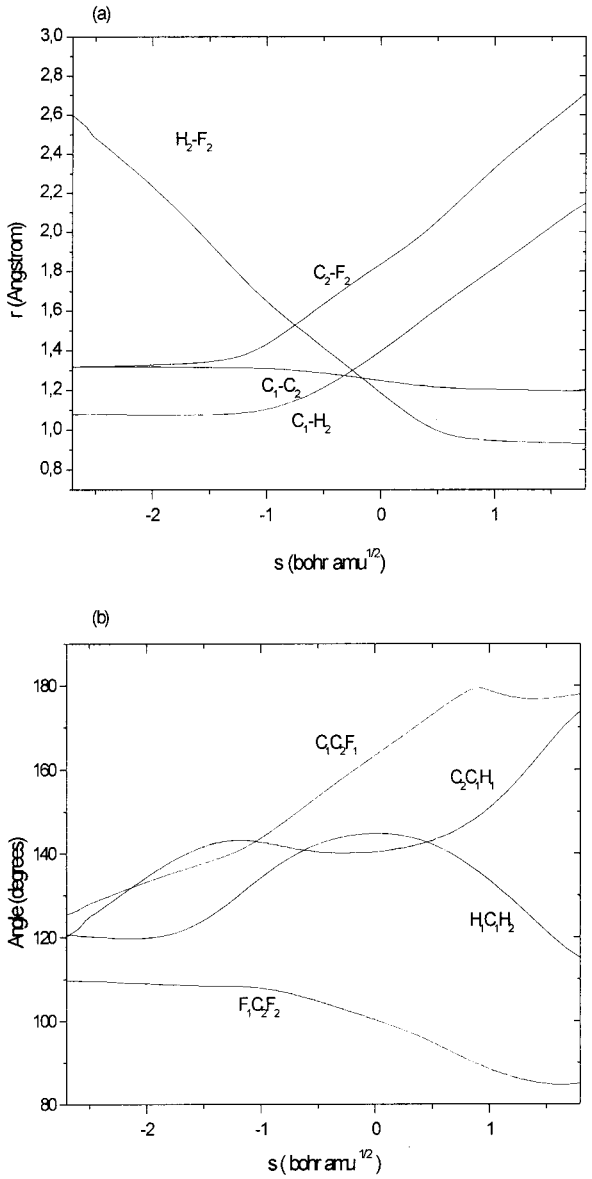

Figure 6. Variation of (a) bond lengths and (b) angles along the reaction coordinate at B3PW91/B3.

Rate Coefficient Calculation. Conventional transition state theory (TST) overestimates the rate coefficient, because it assumes that all trajectories passing through the dividing surface go on to products without recrossing. Therefore, the best choice of the dividing surface is one that minimizes the rate coefficient. This is the assumption of the variational transition state theory.[26] In the canonical approach to this theory (CVT) the criterion for determining the position of the transition state is referred to as the maximum free energy criterion, maximum $\Delta G^{\ddagger}$.

In Table 5 the variational effects for each calculated reaction path are presented. These values are denominated bottleneck properties. In all the results, the variational transition state's position shifts to the reagent region. As expected, the variational transition state is located in the vicinity of the chemical barrier. At lower temperatures the enthalpy change $\Delta H^{\ddagger}$ dominates and favors a maximum in $\Delta G^{\ddagger}$ in the vicinity of the enthalpy maximum ($s = 0.0$). The contribution of the $\Delta S^{\ddagger}$ term to the free energy becomes more important as the temperature increases. Hence, the position of the optimum canonical variational transition state moves to smaller separation of the fragments (i.e., to the reactant region) with increasing temperature.

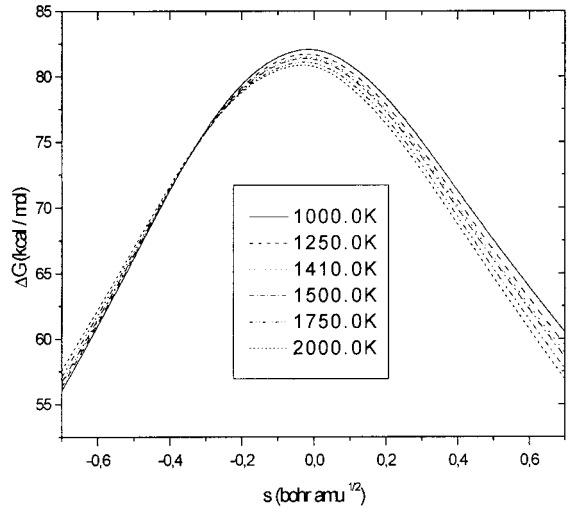

Figure 7. Variation of the free energy of activation as a function of the reaction coordinate *s*. These results were calculated at the B3PW91/B3 level.

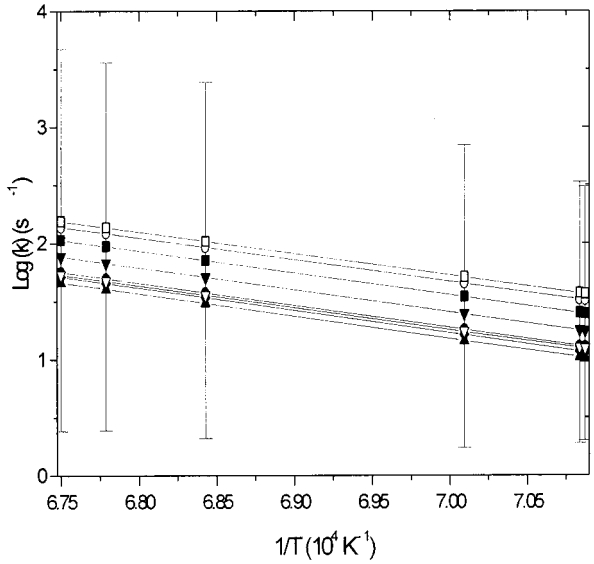

Figure 8. Rate coefficients calculated using the variational transition state theory and different levels to evaluate the reaction path. Symbols: (■) B3PW91/B2; (●) B3PW91/B1; (▲) MP2/B1; (▼) B3LYP/B1 (◆) MP2/B2; (▽) B3PW91/B3; (○) B3LYP/B2; (□) B3LYP/B3. The experimental results are represented by error bars.

Figure 7 shows the generalized standard-state free energy calculated as a function of *s* for several temperatures using the B3PW91/B3 results to determine the potential energy curve. This curve is similar to the potential energy curves (Figure 3), according to the expression $\Delta G^{\ddagger} = \Delta H^{\ddagger} - T\Delta S^{\ddagger}$, and clearly reflects that the $\Delta G^{\ddagger}$ maximum moves to negative values of *s* as the temperature increases.

Table 6 lists the conventional (TST), the variational (CVT and ICVT), and the experimental rate coefficients for the temperature range 1000−1500 K. In this table, the small difference between conventional and variational rate coefficients can be observed.

Figure 8 shows the Arrhenius plots for the rate coefficients calculated by CVT together with the experimental result represented by the error bars.

In the above figures and the tables, it can be seen that the calculated results differ from the experimental rate coefficients by a factor of 0.73−3.5. These results also show that the B3PW91/B3 and B3LYP/B3 data give different rate coefficients,

TABLE 5: Bottleneck Properties Based on the CVT Method with s in Units of bohr amu$^{1/2}$ and V_{MEP} in kcal/mol

	1000 K	1250 K	1411 K	1414 K	1428 K	1463 K	1476 K	1482 K	1500 K
					MP2/B1				
s	−0.0089	−0.0112	−0.0127	−0.0127	−0.0129	−0.0132	−0.0133	−0.0134	−0.0136
V_{MEP}	90.156	90.150	90.146	90.146	90.145	90.144	90.144	90.144	90.143
					MP2/B2				
s	−0.0147	−0.0183	−0.0205	−0.0205	−0.0207	−0.0211	−0.0213	−0.0214	−0.0217
V_{MEP}	90.035	90.022	90.012	90.012	90.011	90.009	90.008	90.008	90.007
					B3PW91/B1				
s	−0.0260	−0.0291	−0.0308	−0.0308	−0.0309	−0.0312	−0.0314	−0.0314	−0.0316
V_{MEP}	89.204	89.189	89.181	89.181	89.180	89.178	89.178	89.177	89.176
					B3PW91/B2				
s	−0.0162	−0.0196	−0.0216	−0.0217	−0.0218	−0.0223	−0.0224	−0.0225	−0.0227
V_{MEP}	88.092	88.082	88.075	88.075	88.074	88.073	88.072	88.072	88.071
					B3PW91/B3				
s	−0.0146	−0.0179	−0.0199	−0.0200	−0.0201	−0.0205	−0.0207	−0.0208	−0.0210
V_{MEP}	88.227	88.217	88.211	88.211	88.210	88.209	88.209	88.208	88.207
					B3LYP/B1				
s	−0.0148	−0.0180	−0.0199	−0.0200	−0.0201	−0.0205	−0.0207	−0.0208	−0.0210
V_{MEP}	88.718	88.709	88.703	88.703	88.702	88.701	88.700	88.700	88.699
					B3LYP/B2				
s	−0.0201	−0.0235	−0.0256	−0.0257	−0.0258	−0.0263	−0.0265	−0.0266	−0.0268
V_{MEP}	87.636	87.625	87.618	87.617	87.167	87.615	87.614	87.614	87.613
					B3LYP/B3				
s	−0.0161	−0.0197	−0.0219	−0.0219	−0.0221	−0.0226	−0.0228	−0.0229	−0.0231
V_{MEP}	87.045	87.034	87.026	87.026	87.025	87.023	87.023	87.022	87.021

TABLE 6: Forward Rate Coefficients (s^{-1})

rate coeff	1000 K	1250 K	1411 K	1414 K	1428 K	1463 K	1476 K	1482 K	1500 K
					MP2/B1				
TST	2.7E−05	0.1834	10.41	10.63	14.74	30.78	40.93	46.47	67.30
CVT	2.7E−05	0.1823	10.32	10.53	14.58	30.62	40.64	46.13	66.77
ICVT	2.7E−05	0.1823	10.32	10.53	14.68	30.62	40.64	46.13	66.77
					MP2/B2				
TST	3.1E−05	0.2098	11.92	12.03	16.76	35.05	46.43	52.73	76.44
CVT	3.1E−05	0.2062	11.63	11.83	16.44	34.32	45.51	51.74	74.78
ICVT	3.1E−05	0.2062	11.63	11.83	16.44	34.32	45.51	51.74	74.78
					B3PW91/B1				
TST	4.0E−05	0.2542	13.91	14.13	19.59	40.69	53.90	61.17	88.30
CVT	3.8E−05	0.2374	12.94	13.14	18.21	37.80	50.05	56.79	81.95
ICVT	3.8E−05	0.2374	12.94	13.14	18.21	37.80	50.05	56.79	81.95
					B3PW91/B2				
TST	8.7E−05	0.4882	25.31	25.71	35.49	72.98	96.31	109.1	156.7
CVT	8.6E−05	0.4799	24.83	25.22	34.81	71.56	94.43	106.9	153.6
ICVT	8.8E−05	0.4799	24.83	25.22	34.81	71.56	94.43	106.9	153.6
					B3PW91/B3				
TST	4.1E−05	0.2389	12.61	12.81	17.71	36.54	48.28	54.73	78.73
CVT	4.1E−05	0.2355	12.41	12.61	17.43	35.94	47.48	53.82	77.42
ICVT	4.1E−05	0.2355	12.41	12.61	17.43	35.94	47.48	53.82	77.42
					B3LYP/B1				
TST	5.6E−05	0.3362	17.95	18.24	25.23	52.17	68.99	78.23	112.7
CVT	5.6E−05	0.3311	17.65	17.93	24.81	51.27	67.80	76.88	110.7
ICVT	5.6E−05	0.3311	17.65	17.93	24.81	51.27	67.80	76.88	110.7
					B3LYP/B2				
TST	1.2E−04	0.6552	33.27	33.78	46.55	95.37	125.7	142.3	204.0
CVT	1.2E−04	0.6389	32.38	32.88	45.30	92.77	122.2	138.4	198.3
ICVT	1.2E−04	0.6389	32.38	32.88	45.30	92.77	122.2	138.4	198.3
					B3LYP/B3				
TST	1.5E−04	0.7535	37.34	37.92	52.15	106.4	139.9	158.3	226.4
CVT	1.5E−04	0.7407	36.64	37.20	51.15	104.3	137.2	155.2	221.9
ICVT	1.5E−04	0.7407	36.64	37.20	51.15	104.3	137.2	155.2	221.9
					Experimental Results				
			12.3	13.3	20.1	34.1	38.2	44.1	

despite the agreement between the energy barriers. This suggests that both the vibrational frequencies and the barriers should be considered in the selection of the best level of calculation,[32] once the values of the partition functions along the MEP are very sensitive to the values of the computed frequencies. For the system under investigation, it seems that the MP2 and B3PW91 methods give the best rate coefficient results. Unfortunately, since experimental results have large error bars, it is

very difficult to choose here, from a comparison with experimental data, which is the best method of calculation. Anyway, it is important to emphasize the good values obtained using DFT methods. These results suggest that these methods are reliable for the calculation of the saddle point and reaction path structures and give reasonable results for the barrier height and other systems are being investigated in our laboratory. These methods may be particularly useful for the study of larger species.[33]

As expected, the conventional TST rate coefficients are slightly higher than the canonical variational transition state theory coefficients (CVT). The reason for the rather small difference is that, within the temperature range 1000−1500 K, the localization of variational dividing surface differs by less than 0.03 bohr amu$^{1/2}$ from the saddle point of the potential energy surface ($s = 0.0$). The improved canonical variational results (ICVT) are identical with the CVT results over the temperature range considered, which suggests that the microcanonical variational transition states have weak energy dependence and the canonical variational transition state is a satisfactory average of the transition states for the energies and angular momenta which are most important at each temperature.

Conclusions

The computed results show good agreement, within the uncertainties of the experimental values, for both the critical energy and rate coefficients. Unfortunately, the uncertainty in the experimental critical energy makes it impossible to indicate which of the methods used is the best for the calculation of the reaction barrier and rate coefficients. However, the MP2 and B3PW91 levels of calculation seem satisfactory for the description of this reaction. Higher levels of calculation, such as CCSD(T) and MP4SDQ, give similar results for the critical energy. It can also be noticed that fairly larger bases give lower barrier heights and both the vibrational frequencies and the critical energies should be considered in choosing the best level of calculation for each system.

Acknowledgment. The authors thank the CAPES and CNPq (Conselho Nacional de Desenvolvimento Científico e Tecnológico) for financial support and Prof. Marco Antonio Chaer Nascimento and NCE/UFRJ for computational facilities.

References and Notes

(1) Burgess, D. R., Jr.; Zachariah, Mr. R.; Tsang, W.; Westmoreland, P. R. *Prog. Energy Combust. Sci.* **1996**, *21*, 453.

(2) (a) Atkinson, R.; Pitts, J. N., Jr. *J. Chem. Phys.* **1977**, *67*, 2488. (b) Gilbert, J. R.; Slagle, I. R.; Graham, R. E.; Gutman, D. *J. Phys. Chem. Ref. Data* **1987**, *16*, 261. (c) Herron, J. T.; Huie, R. E. *J. Phys. Chem. Ref. Data* **1973**, *2*, 467. (d) Jones, D. S.; Moss, S. J. *Int. J. Chem. Kinet.* **1974**, *6*, 443.

(3) March, J. *Advanced Organic Chemistry*, 4th ed.; John Wiley & Sons: New York; Chapter 17.

(4) Simmie, J. M.; Tschuikow-Roux, E. *J. Phys. Chem.* **1970**, *74*, 4075.

(5) (a) Macoll, A. *Chem. Rev.* **1969**, *69*, 33. (b) Sianesi, D.; Nelli, G.; Fontanelli, R. *Chim. Ind.* **1968**, *50*, 619. (c) Day, M.; Trotman-Dickenson, A. F. *J. Chem. Soc. A* **1969**, 233. (d) Cadman, P.; Day, M.; Kirk, A. W.; Trotman-Dickenson, A. F. *Chem. Commun.* **1970**, 203. (e) Simmie, J. M.; Quiring, W. J.; Tschuikow-Roux, E. *J. Phys. Chem.* **1970**, *74*, 992.

(6) Strausz, O. P.; Norstrom, R. J.; Salahub, D.; Goravi, R. K.; Gunning, H. E.; Crizmadia, I. G. *J. Am. Chem. Soc.* **1970**, *92*, 6395.

(7) Clough, P. N.; Polanyi, J. C.; Taguchi, R. T. *Can. J. Chem.* **1970**, *48*, 2919.

(8) Watanabe, H.; Horiguchi, H.; Tsuchiya, S. *Bull. Chem Soc. Jpn.* **1980**, *53*, 1530.

(9) Quick, C. R., Jr.; Wittig, C. *J. Chem. Phys.* **1980**, *72*, 1694.

(10) Riehl, J.-F.; Musaev, D. G.; Morokuma, K. *J. Chem. Phys.* **1994**, *101*, 5942.

(11) Resende, S. M.; Almeida, W. B. *Chem. Phys.* **1998**, *238*, 11.

(12) (a) Fukui, K. *J. Phys. Chem.* **1970**, *74*, 4161. (b) Truhlar, D. G.; Kupermann, A. J. *J. Am. Chem. Soc.* **1971**, *93*, 1840. (c) Fukui, K. *Pure Appl. Chem.* **1982**, *54*, 1825.

(13) (a) Baldridge, K. M.; Gordon, M. S.; Steckler, R.; Truhlar, D. G. *J. Phys. Chem.* **1989**, *93*, 5107. (b) Truhlar, D. G.; Gordon, M. S. *Science* **1990**, *249*, 491.

(14) Silva, A. M. M.Sc. Thesis, 1999.

(15) Frisch, M. J.; Trucks, G. W.; Schlegel, H. B.; Gill, P. M. W.; Johnson, B. G.; Robb, M. A.; Cheeseman, J. R.; Keith, T. A.; Petersson, G. A.; Montgomery, J. A.; Raghavachari, K.; Al-Laham, M. A.; Zakrewski, V. G.; Ortiz, J. V.; Foresman, J. B.; Cioslowski, J.; Stefanov, B. B.; Nanayakkara, A.; Challacombe, M.; Peng, C. Y.; Ayala, P. Y.; Chen, W.; Wong, M. W.; Andres, J. L.; Replogle, E. S.; Gomperts, R.; Martin, R. L.; Fox, D. J.; Binkley, J. S.; Defrees, D. J.; Baker, J.; Stewart, J. P.; Head-Gordon, M.; Gonzales, C.; Pople, J. A. *Gaussian 94 (Revision E.2)*; Gaussian, Inc.: Pittsburgh, PA, 1995.

(16) Schmidt, M. W.; Baldridge, K. K.; Boatz, J. A.; Elbert, S. T.; Gordon, M. S.; Hensen, J. H.; Koseki, S.; Matsunaga, N.; Nguyen, K. A.; Su, S. J.; Windus, T. L.; Dupuis, M.; Montgomery, J. A. *J. Comput. Chem.* **1993**, *14*, 1347.

(17) MØller, C.; Plesset, M. S. *Phys. Rev.* **1934**, *46*, 618.

(18) (a) Lee, C.; Yang, W.; Parr, R. G. *Phys. Rev.* B **1988**, *37*, 785. (b) Becke, A. D. *J. Chem. Phys.* **1993**, *98*, 5648.

(19) (a) Perdew, J. P.; Chevary, J. A.; Vosko, S. H.; Jackson, K. A.; Peserson, M. R.; Singh, D. J.; Fiolhais, C. *Phys. Rev.* B **1992**, *46*, 6671; *Phys. Rev.* B **1993**, *48*, 4978.

(20) (a) Pople, J. A.; Seeger, R.; Krishnan, R. *Int. Quantum Chem. Symp.* **1977**, *11*, 149. (b) Krishnan, R.; Schlegel, H. B.; Pople, J. A. *J. Chem. Phys.* **1980**, *72*, 4654.

(21) (a) Schlegel, H. B.; Robb, M. A. *Chem. Phys. Lett.* **1982**, *93*, 43. (b) Bernardi, F.; Bottini, A.; McDougall, J. J.; Robb, M. A.; Schlegel, H. B. *Faraday Symp. Chem. Soc.* **1984**, *19*, 137.

(22) Dunning, T. H., Jr.; Hay, P. J. In *Modern Theoretical Chemistry*; Schaefer, H. F., III, Ed.; Plenum: New York, 1976; p 1.

(23) (a) Woon, D. E.; Dunning, T. H., Jr. *J. Chem. Phys*. **1993**, *98*, 1358. (b) Kendall, R. A.; Dunning, T. H., Jr.; Harrison, R. J. *J. Chem. Phys.* **1992**, *96*, 6796. (c) Dunning, T. H., Jr. *J. Chem. Phys.* **1989**, *90*, 1007.

(24) Miller, W. H.; Handy, N. C.; Adams, J. E. *J. Chem. Phys.* **1980**, *72*, 99.

(25) Chuang, Y.-Y.; Coitiño, E. L.; Hu, W.-P.; Liu, Y.-P.; Lynch, G. C.; Nguyen, K. A.; Jackels, C. F.; Gu, M. Z.; Rossi, I.; Fast, P.; Clayton, S.; Melissas, V. S.; Garret, B. C.; Isaacson, A. D.; Truhlar, D. G. *POLYRATE*, version 7.0; University of Minneapolis: Minneapolis, MN, 1996.

(26) Gilbert, R. G.; Smith, S. C. *Theory of Unimolecular and Recombination Reactions*; Blackwell Scientific Publications: Oxford, U.K., 1990; Chapter 3.

(27) Laurie, V. W.; Pence, D. T. *J. Chem. Phys.* **1963**, *38*, 2693.

(28) Carlos, J. L.; Karl, R. R.; Bauer, S. H. *J. Chem. Soc., Faraday Trans. 2* 1974, *70*, 177.

(29) Huber, K. P.; Herzberg, G. *Constants of Diatomic Molecules*; Van Nostrand Reinhold: New York, 1979.

(30) Tyler, J. K.; Sheridan, J. *Trans. Faraday Soc.* **1963**, *59*, 2661.

(31) Mckean, D. C. *Spectrochim. Acta, Part A* 1975, *31A*, 1167.

(32) Bauerfeldt, G. F.; Arbilla, G.; Silva, E. C. *J. Phys. Chem. A*, submitted for publication.

(33) Abashkin, Y.; Russo, N.; Toscano, M. *Int. J. Quantum Chem.* **1994**, *52*, 695.